International Journal of Scientific Research and Reviews

Impedance Spectroscopy of ZnS Nanoparticles Embedded in Conducting Polymer

Dutta Kousik[*]

Department of Physics, Behala College, Parnashree; Kolkata- 700060; INDIA
(Dated: August 20, 2018)
Author for correspondence : (Tel: +91-33-9434575658;
E-mail: duttakousik2003@yahoo.co.in)

ABSTRACT

Complex impedance and dielectric permittivity of zinc sulphide (ZnS) -conducting polyaniline (PANI) nanocomposite have been investigated as a function of frequency and temperature at different compositions. Inorganic -organic hybrid nanocomposites are synthesized by dispersing nanosized ZnS in the conducting polyaniline (PANI) matrix. Grain and grain boundary contributions are observed in the impedance spectra. The results are interpreted in terms of two series connected equivalent circuit. The dielectric permittivity 2400 is found for the sample with highest content of nanosized zinc sulphide (ZnS). Large value of permittivity is well described by Maxwell-Wagner polarization. Broad and asymmetric dielectric spectra are analyzed by Harviliak - Nigami relaxation function.

KEYWORDS: Conducting polymer, ZnS nanoparticles, nanocomposites, dielectric properties

*Corresponding author

Kousik Dutta

Department of Physics,

Behala College, Parnashree; Kolkata- 700060; INDIA

Tel: +91-33-9434575658, E-mail: duttakousik2003@yahoo.co.in

INTRODUCTION

The fabrication of complex nano architectures with controlled morphology and dimensionality have attracted significant attention over the past decades since such control is crucial for the determination of structure dependent properties in many processes, development of new path ways for the material synthesis and novel application of nanostructure materials. [1 - 3] It is well known that electronic and optical properties of nanocrystalline semiconductor exhibits intriguing features comparison to the bulk due to quantum size effect. Nanosized materials possesses properties that are different from bulk materials. Control over both nanocrystalline morphology and particle size by different synthesis routes enables the researchers to obtain desire properties for the purpose of application. Semiconductor nanoparticles have attracted much interest due to their fundamental as well as technological importance. Nanocomposites are the special class of materials in which at least one component has nanosized dimension [4] The investigation of polymer-inorganic nanocomposite is motivated by many reasons, including the need for novel electronic anisotropic materials, better performing battery, functionalize structural materials with superior mechanical and thermal properties. It is therefore expected that these type of materials will play increasingly important role in research and have numerous application in the various field of nanoscience industry.

Recently, low dimensional nanostructured materials, such as nanotubes, nanorods and nanowires have attracted considerable interest because of their unique physical and electrical properties and potential applications in optics, magnetics and electronics. [5, 6] Among the family of II-VI group semiconductor nanomaterials such as CdS [7, 8] ZnS, [9, 10] CdSe [4], ZnO [11], CdTe [12] are the fore most candidates because of their electronic and electrical properties for optoelectronic application. As an important semiconductor with a direct wide band gap of 3.8 eV, Zinc Sulphide has attracted considerable research interest due to the intense usage in electroluminescent devices, at panel displays, infrared windows, sensors, and lasers. [13, 14] The electronic properties of nanosized ZnS are also strongly influenced by doping of transition and rare earth metals. [15, 16] The emission efficiency and thermal stability are increased upon reduction of ZnS particle size. [17 - 19] Various chemical and physical technique are employed to investigate the optical properties of nanocrystalline ZnS. [20 - 22] The confinement of electrons within nano dimension leads to unusual behavior. The combination of inorganic and organic species generates new materials for the development of new multifunctional devices. Hybrid II-VI semiconductor nanocomposites are formed through chemical bonding with organic substance. [23 – 25] Dispersion of inorganic nanoparticles in the polymer matrix is a novel route to synthesize hybrid inorganic-organic nanocomposites. Polyaniline is an intrinsically conductive polymer of any conductive substances. Extensive research activities on PANI have been

performed because of high conductivity. [26] Mutual interactions between inorganic semiconductor and organic polymers may give rise to interesting properties which are significantly different from individual components. In the present work, it is reported that synthesis of conducting polyaniline (PANI) in the presence of ZnS nanoparticles to investigate dielectric properties by varying the concentration of nanocomposite.
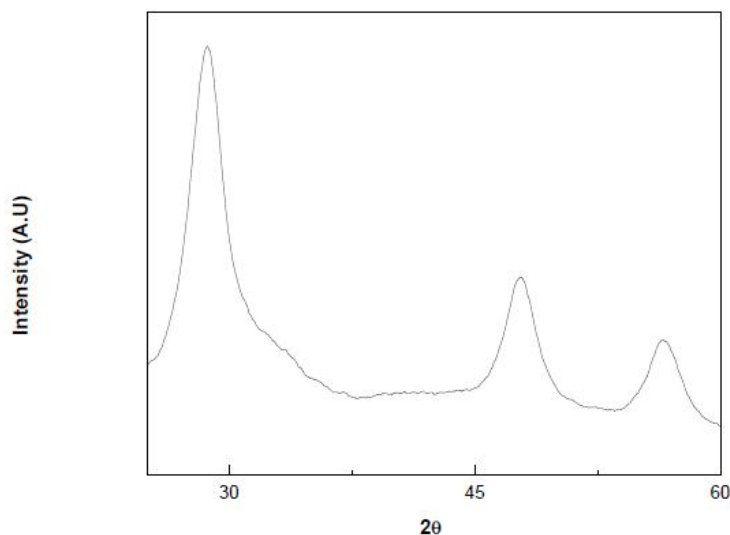

FIG. 1: X-ray diffraction pattern of ZnS-PANI nanocomposite sample S1.

EXPERIMENTAL

Synthesis of a material is a vital part of material research, because proper tailoring is necessary to make a material interesting in properties. Of the different methods of preparation, chemical method of preparation of nanomaterial is more advantageous because of good control over stoichiometry of the reactants is obtained. In this research work all the chemicals used were of analytical grade. Aniline and ammonium peroxydisulphate (APS) $((NH_4)_2S_2O_8)$ were obtained from E. Merck (India). Aniline (AR grade) was purified and stored at -15^0 C in a refrigerator prior to use. APS oxidant was used as received.
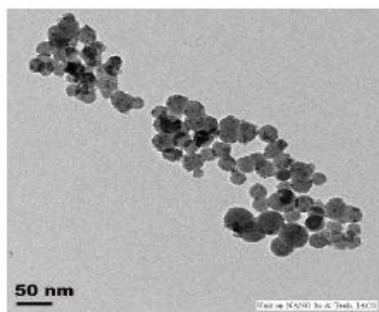
FIG. 2: TEM micrograph of lower magnification image of nanocomposites sample S4.

ZnS nanoparticle were synthesized by a standard chemical technique. [27] In a typical synthesis 1.75 gm of Zinc perchlorate ($Zn(ClO_4)_2$) was dissolved in 250 ml of deionized water and stirred for 1 hour at room temperature. Aqueous solution of thioglycerol (12mM) was mixed drop wise with the aqueous solution of Zinc Perchlorate under constant stirring.
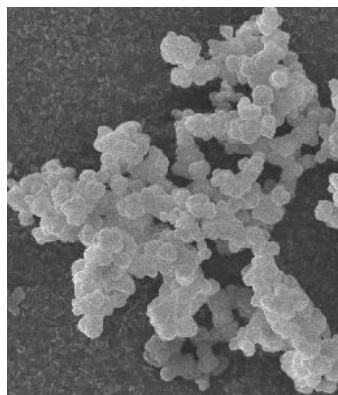

FIG. 3: Scanning electron micrographs of nanocomposites sample S1.

The pH of the resultant solution was kept at 11 with the addition of NaOH aqueous solution. After 45 minutes Na_2S solution was mixed slowly with the above reaction mixture and stirred for 1 hours at 80^0 C and to cool to room temperature. The solution was dialyzed against water and then concentrated and mixed with 2- propanol to make as a precipitate. Finally the resultant nanoparticles were washed several times with methanol to remove the unwanted impurities and dried in a vacuum oven at 70^0 C for 6 hour. The required quantity of ZnS nanoparticle was ultrasonically dispersed in 50 ml deionized water. Aniline monomer of known volume was slowly added into the dispersion under sonication at room temperature. Then the aqueous solution of APS maintaining a aniline : APS mole ratio of 1:1.25 was added drop wise into the previous deionized water containing nanosized

ZnS and aniline monomer. After few hours the resulting solution was turned into green color which indicates the formation of polyaniline. The solution was then kept under sonication for about 6 hours to ensure complete polymerization. Finally the resulting green dispersion were centrifuged. The resulting nanocomposites were washed thoroughly with distilled water for several times. Different compositions of nanocomposite samples with varying the weight percentage of aniline (polyaniline) were prepared as shown in Table I. The samples were pressed into pellets of diameter 1 cm. The thickness of the samples varies from 0.10 cm to 0.12 cm.
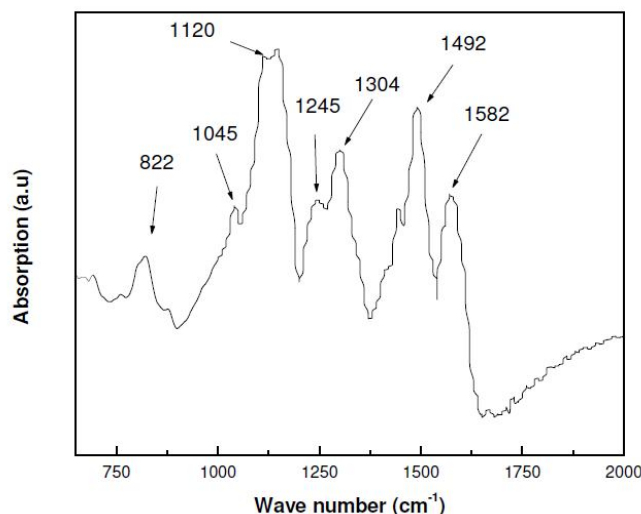

FIG. 4: Fourier Transform Infrared (FTIR) spectra of sample S1.

X ray diffraction pattern of the nanocomposites were performed using a Philips Difractrometer (PW1710) with Cuk$_\alpha$ radiation. Scanning electron microscope (SEM) (Model JEOL JSM6700F) image was obtained using scanning electron microscope. Transmission electron micrographs were taken from JEOL, TEM 2010. The capacitance (C) and loss factor (D) as a function of frequency were measured by Agilent 4192A impedance analyzer up to the frequency range 10 MHz at different temperatures. The real part of the ac conductivity σ (ω) was determined by the relation σ (ω) = ω DCt/A, where t is the thickness and A is the area of the sample. The electrical contacts were made by silver paint.

RESULTS AND DISCUSSION

Figure 1 displays the powder X-ray diffraction (XRD) of the sample S1. The wide angle XRD pattern for the bulk system exhibits three distinct peaks in the range of 2 θ = 20 - 60^0, characteristics of the cubic structure. The peaks are fairly broad suggesting the nanostructure of ZnS. The three strong peaks appeared at angles (2 θ) of 28.7, 47.7, 56.6 correspond to 111, 220 and 311 planes of cubic ZnS. Two crystalline polymorphs of

TABLE 1: Weight percentage of polyaniline (x), activation energy from grain boundary (E$_{gb}$) and grain (E$_g$) conductivity and activation energy E$_\tau$ of dielectric relaxation, real part of relative dielectric permittivity (ε$_1$) at room temperature (RT)

Sample	x	Egb (meV)	Eg (meV)	Eτ (meV)	ε$_1$ (RT)
S1	74	66	45	47	1680
S2	61	75	56	58	1950
S3	48	84	69	73	2170
S4	35	96	85	83	2400

ZnS are found: cubic zincblende (saphlerite) and hexagonal (wurtzite). Cubic phase is the most stable phase at ambient condition. Hexagonal structure is formed at highest temperature (>1200 K). The present XRD pattern matches well with the reported cubic phase of ZnS. The mean size (D) of ZnS nanoparticles of the nanocomposite is calculated following the Scherer's equation [28]

$$D = K\lambda/\beta \cos \theta \qquad (1)$$

where K = 0.89, D represents coherent length, λ, the wavelength of Cu k$_\alpha$ radiation and β, the corrected value at full width at half maxima (FWHM) of the diffraction peak. At $2\theta = 28.7°$, which is the characteristics peak of ZnS, is chosen to calculate D. The estimated size of nanocrystalline ZnS is 5.1 nm.

Figure 2 shows the TEM micrograph of the ZnS-polyaniline nanocomposites particle. In this micrographs nearly spherical crystallites are observed. The mean particle size of pure ZnS is in the range of 5-8 nm which is good agreement with XRD result. TEM of nanocomposite S4 in Figure 2 depicts larger particle size having 20-30 nm. Larger particle size may be due to the aggregation of smaller particles in the presence of polymer matrix.

The scanning electron micrograph (SEM) of the nanocomposite sample S1 is shown in Figure 3. The nanocomposite particles are well dispersed and are of spherical shape with uniform diameter lying in the range from 25- 30 nm
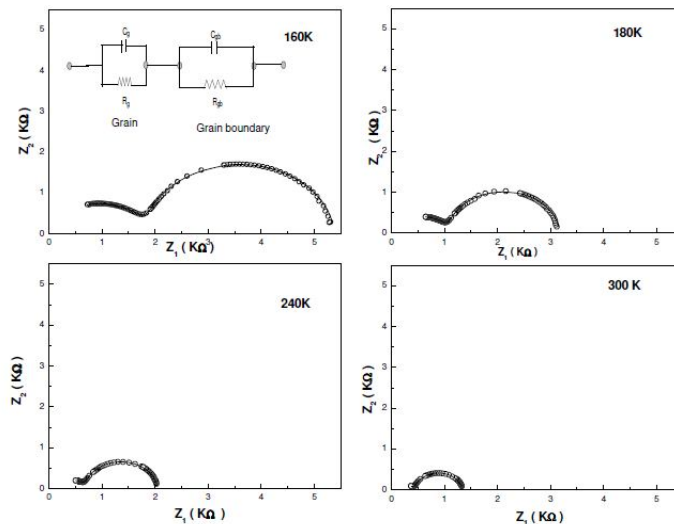
FIG. 5: Impedance spectra of the sample S4 at four different temperatures. The solid lines are fits to the proposed equivalent circuit for the sample.

A typical FTIR spectrum of the nanocomposite sample S1 is illustrated in Figure 4. The bands at 1582 and 1492 cm^{-1} are attributed to C=N and C=C stretching mode of vibration for the quinonoid and benzenoid units of polyaniline. The peaks at 1304 and 1245 cm^{-1} are assigned to C - N stretching mode of benzenoid ring. The peak at 1245 cm^{-1} is the characteristic of the conducting form of polyaniline. The bands in the region 1000 – 1200 cm^{-1} are due to in plane bending vibration of C-H mode. The band at 822 cm^{-1} originates out of plane C-H bending vibration. The typical FTIR spectrum of PANI is consistent with the previous results. [29, 30] Almost all the bands reveal blue shift in the nanocomposites which indicates that there is a strong interaction between polyaniline and ZnS nanoparticles.

Figure 5. represents the complex impedance, $Z = Z_1 + iZ_2$ plots for the sample S4 at different temperatures. At room temperature, two incomplete semicircles are observed. The high frequency contribution dominates with lowering of temperature. The features of the impedance spectra of polycrystalline composite materials primarily depend on the microstructure. The SEM micrographs indicate that the nanocomposites consist of nanometer size grains which introduce more grain boundaries within the samples. The impedance spectra can be interpreted by the equivalent circuit consisting of series connected parallel resistance (R) and capacitance (C) components as shown in Figure 5.
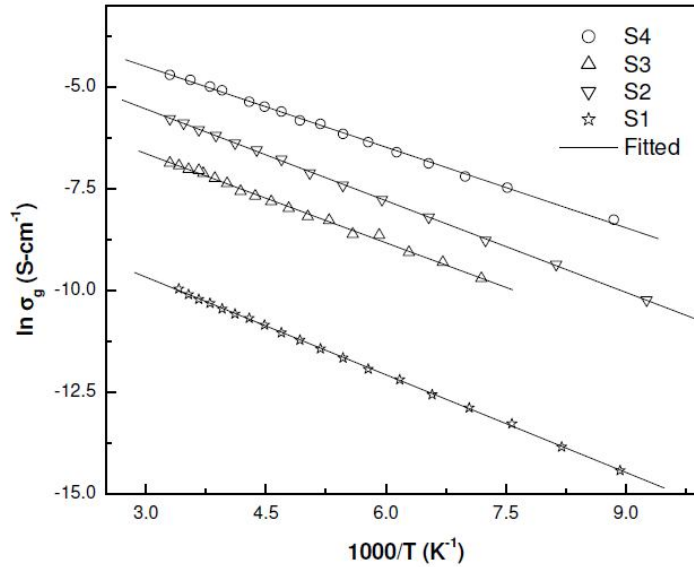
FIG. 6: Arrhenius plot of grain conductivity for the four different samples.

The position of the maximum arc in the impedance diagram is determined by the relation $\omega_{max}RC = 1$, where $\omega_{max} = 2\pi f$, f is the applied frequency. The larger values of R and C at grain boundary lead to smaller ω_{max} compared to grain. Moreover, ω_{max} lies outside the available frequency range and only some portions of semicircles are obtained at higher temperature. The grain and grain boundary responses are analyzed by the following relations

$$Z_1 = \frac{R_g}{1 + (\omega R_g C_g)^2} + \frac{R_{gb}}{1 + (\omega R_{gb} C_{gb})^2} \quad (2)$$

$$Z_2 = R_g \left[\frac{\omega R_g C_g}{1 + (\omega R_g C_g)^2} \right] + R_{gb} \left[\frac{\omega R_{gb} C_{gb}}{1 + (\omega R_{gb} C_{gb})^2} \right] \quad (3)$$

where (R_g, R_{gb}) and (C_g, C_{gb}) are resistance and capacitance of grain and grain boundary respectively. Equations (2) and (3) represent two ideal semicircles whose centers lie on the real Z1 axis. The constant phase elements (CPE) capacitors $C(\omega) = B(i\,\omega)^{n-1}$ are assumed to analyze the more flattened semicircles [31, 32]. The parameter B is constant for a given set of experimental data. The exponent n varies between 0 and 1. The impedance of CPE behaves as an ideal capacitor for n = 1 and ideal resistor for n = 0. The experimental data are best fitted employing complex nonlinear curve fitting LEVM program developed by Macdonald [33]. The solid lines in Figure 5 represent the best fitted calculated values. Both C_{gb} and C_g are weak temperature dependent.

Grain (σ_g) and grain boundary (σ_{gb}) conductivities have been calculated from the best fitted values of R_g and R_{gb}. Figures 6 and 7 show the temperature dependence of grain and grain boundary conductivity. The estimated grain boundary conductivity is about 100 times lower than that of grain

conductivity. Both σ_g and σ_{gb} follow Arrhenius type process with temperature as evidence from the plots in Figures 6 and 7.
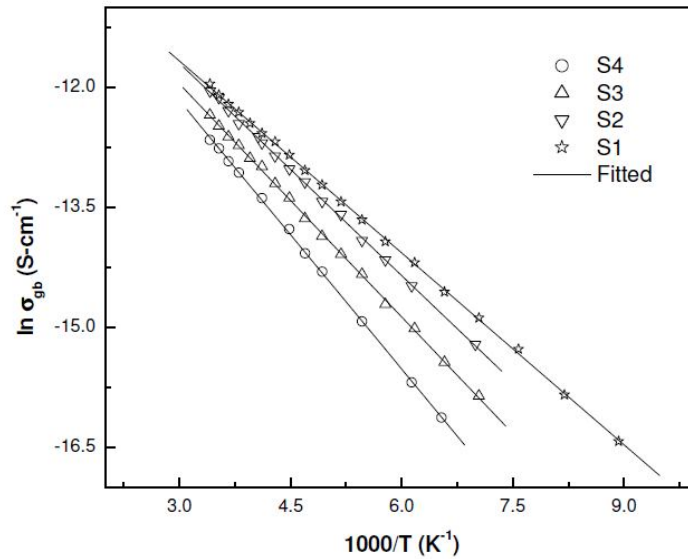

FIG. 7: Arrhenius plot of grain boundary conductivity for the different samples.

The activation energies are derived from the slopes of the straight lines as shown in Table I. The activation energy of the grain interior is smaller than that of grain boundary. The conductivity of grain boundary region is mainly determined by the microstructure. The temperature dependence of conductivity of PANI obeys Mott's three dimensional variable range hopping process**.** [26, 34] Thermally activated conductivity variation suggests that PANI is not dominating the conduction process.
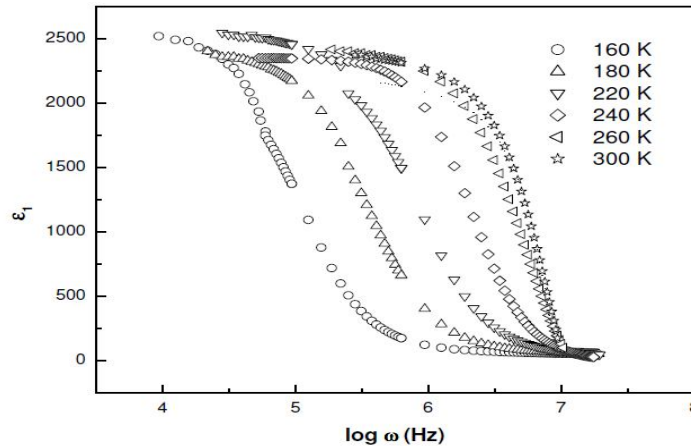

FIG. 8: Frequency dependence of the real part of relative dielectric constant (ε_1) at different temperatures for the sample S4.

The value of ε_1 decreases with decrease of ZnS content. At high frequency greater than 10 MHz, ε_1 reaches to about 60. Figures 8 represents the temperature dependence of ε_1 for S4. The high frequency value of ε_1 is almost independent of temperature. The unusually large dielectric constant can be explained by interfacial Maxwell-Wagner (MW) interfacial relaxation commonly applied in heterogeneous system. The nanocomposites consist of conducting grains and resistive grain boundaries. Under the application of external electric field, the charge carriers can easily migrate the grains but are accumulated at the grain boundaries. This process can produce large polarization and high dielectric constant. The small conductivity of grain boundary contributes to high value of dielectric constant at low frequency. The static dielectric constant based on the equivalent circuit in Figures 5 can be expressed as

$$\epsilon^* = \epsilon_\infty + \frac{\epsilon_s - \epsilon_\infty}{(1 + (i\omega\tau)^\beta)^\alpha} \qquad (4)$$

Resistance and capacitance of grain boundary are much larger than that of grain. In MW polarisation, dielectric constant under such condition can be approximated from eq.(4) as $\varepsilon_1(0) = C_{gb}/C_0$. A large value of C_{gb} leads to very high value of dielectric constant. The ratio of ZnS and PANI modifies the microstructure i.e. grain boundary capacitance. This may be the possible reason for different values of ε_1 for different compositions. The dielectric loss spectra ε_2 as a function of frequency for S4 are shown in Figures 9 for different temperatures. The relaxation peak in the measured frequency domain is appeared at room temperature. The positions of the peaks move to lower frequency with the decrease of temperature. The dielectric response has been analyzed by the most generalized Havriliak-Negami (HN) function [35.]

$$\epsilon^* = \epsilon_\infty + \frac{\epsilon_s - \epsilon_\infty}{(1 + (i\omega\tau)^\beta)^\alpha} \qquad (5)$$

where τ is the average relaxation time which is given at the frequency of maximum dielectric loss. The difference $\Delta\varepsilon = \varepsilon_s - \varepsilon_\infty$ is known as the dielectric relaxation strength. The parameter β describes the distribution of the relaxation time of the system. Debye relaxation is obtained for $\alpha = 1$ and $\beta = 1$. The parameters α and β ranging between 0 and 1 are symmetric and asymmetric broadening of dielectric spectra. The solid lines in Figures 9 show that the experimental data are reasonably good fitted with the calculated value of HN function.

The value of β is different from unity which implies non-Debye relaxation process. This parameter manifests that the dielectric dispersion has a broad distribution of relaxation time. The dielectric strength $\Delta\,\varepsilon$ increases with increase of temperature. The relaxation times, τ at different temperatures are obtained from the best fitted data to eqn. (5).
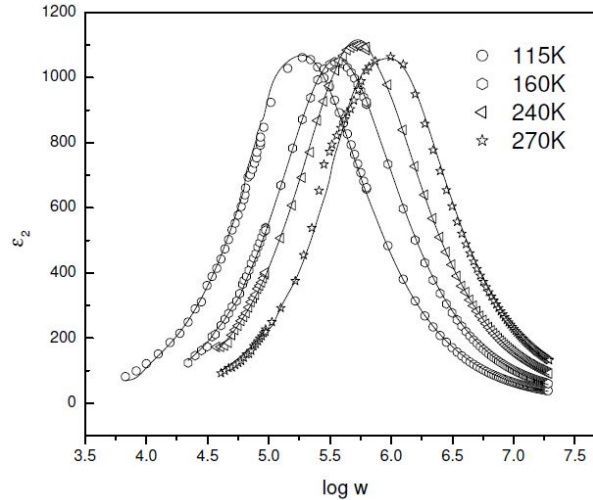

FIG. 9: Frequency dependence of imaginary component of dielectric constant (ε_2) at selected temperatures for the sample S4. The solid lines are fits to Eq.4.

The linear behavior of the Arrehenius plot of ln τ against 1/T suggest that the temperature variation of τ can be described by thermally activated Arrhenius law,

$$\tau = \tau_0 exp(E_\tau/kT) \qquad (6)$$

where τ_0 is the relaxation time at high temperature, E_τ is the activation energy of dielectric process and k is Boltzmann constant. The slope of the best fitted straight line gives the activation energy as shown in Table I. The most interesting fact is that the activation energies are in excellent agreement with the values obtained from grain conductivity.

CONCLUSION

Impedance data demonstrate the existence of electrically semiconducting grains and more resistive grain boundaries. The values of dielectric constant exhibit large variations with compositions, temperature and frequency. The dielectric response at the lower frequency is characterized by Maxwell-Wagner relaxation. The variations of microstructure with compositions render different dielectric constants.

REFERENCES

1. Hu JT, Odom TW, and Lieber CM, Chemistry and Physics in One Dimension: Synthesis and Properties of Nanowires and Nanotubes. J. Am. Chem. Soc. 1999; 32(5): 435-445

2. Law M, Goldberg J, and Yang PD, Semiconductor nawires and nanotubes. Annu. Rev. Mater. Res. 2004; 34: 83-122

3. Yuan JK, Li WN, Gomez S, and Suib SL, Shape-Controlled Synthesis of Manganese Oxide Octahedral Molecular Sieve Three-Dimensional Nanostructures. J. Am. Chem. Soc. 2005; 127 (41): 14184 -14185

4. Beecreft LL, Ober CK, Nanocomposite Materials for Optical Applications. Chem. Matter. 1999; 9(6): 1302 - 1317

5. Peng XG, Manna L, Yang WD, Wickham J, Scher E, Kadavanich A, Alivisatos AP, Shape control of CdSe nanocrystals. Nature. 2000; 404: 59 - 61

6. Kim F, Kwan S, Akana J, Yang PD, Langmuir−Blodgett Nanorod Assembly. J. Am. Chem. Soc. 2001; 123(18): 4360 - 4361

7. Priyam A, Chatterjee A, Das SK, Saha A, Res. Chem Intermed. 2005; 31: 691 - 697

8. Priyam A, Chatterjee A, Das SK, Saha A, Size dependent interaction of biofunctionalized CdS nanoparticles with tyrosine at different pH. Res. Chem Commum. 2005; 32: 4122 - 4124

9. Crounch D, Norager S, Brien PO, Park JH, Pickett N, New synthetic routes for quantum dots. Philos. Trans. R. Soc. A. 2003; 361(1803): 297-310

10. Vogel W, Borse PH, Deshmukh N, Kulkarni SK, Structure and Stability of Monodisperse 1.4-nm ZnS Particles Stabilized by Mercaptoethanol. Langmuir. 2000; 16(4): 2032 -2037

11. Brossmann Ulrich and Würschum Roland Oxygen diffusion in ultrafine grained monoclinic ZrO2. J. Appl. Phys. 1999; 85: 7646 - 7652

12. Rogach AL. Nanocrystalline CdTe and CdTe(S) particles: wet chemical preparation, size-dependent optical properties and perspectives of optoelectronic applications. Mater. Sci. Eng. B 2000; 69-70: 435-440

13. Prevenslik TV, Acoustoluminescence and sonoluminescence, Lumin. J. 2000; 87-89: 1210-1212

14. Calandra P, Goffredi M, and Liveri VT, Study of the growth of ZnS nanoparticles in water/AOT/n-heptane microemulsions by UV-absorption spectroscopy. Colloids Surf. A. 1999; 160 (1) : 9-13

15. Li YQ, Zapien JA, Shan YY, Liu YK and Lee ST, Manganese doping and optical properties of ZnS nanoribbons by postannealing. Appl. Phys. Letts. 2006; 88: 013115-013119

16. Sapra S, Prakash A, Ghangrekar A, Periasamy N. and Sarma D. D, J. Phys. Chem. B. 2005; 109: 1663-1670

17. Bhargava RN, and Gallagher D, Optical properties of manganese-doped nanocrystals of ZnS Phys. Rev. Lettr. 1994; 72: 416-422

18. Bol AA and Meijerink A. Luminescence Quantum Efficiency of Nanocrystalline ZnS:Mn^{2+}. 2. Enhancement by UV Irradiation. J. Phys. Chem. B, 2001; 105: 10203-10209

19. Zhang Y and Li Y. Synthesis and Characterization of Monodisperse Doped ZnS Nanospheres with Enhanced Thermal Stability. J. Phys. Chem. B, 2004; 108(46): 17805-17811

20. Shen G, Bando Y and Golberg D, High-symmetry ZnS hepta- and tetrapods composed of assembled ZnS nanowire arrays. Appl. Phys. Lett. 2007; 90: 123101- 123107

21. Jiang X, Xie Y, Liu J, Zhu L, He W. and Qian Y. Simultaneous In Situ Formation of ZnS Nanowires in a Liquid Crystal Template by γ-Irradiation. Chem. Mater. 2001; 13: 1213-1217

22. Dhas A, Zaban A and Gedanken A. Surface Synthesis of Zinc Sulfide Nanoparticles on Silica Microspheres: Sonochemical Preparation, Characterization, and Optical Properties. Chem. Mater. 1999; 11: 806-811

23. Huang X, Heulings HR, Le V and Li J, Inorganic−Organic Hybrid Composites Containing MQ (II−VI) Slabs: A New Class of Nanostructures with Strong Quantum Confinement and Periodic Arrangement. Chem. Mater. 2001; 13(10): 3754 -3759

24. Heullings HR, Huang X, Li J, Yuen T and Lin CL, Mn-Substituted Inorganic−Organic Hybrid Materials Based on ZnSe: Nanostructures That May Lead to Magnetic Semiconductors with a Strong Quantum Confinement Effect. Nano Lett. 2001; 1(10): 521-525.

25. Fan L, Song H, Zhao H, Pan C, Yu H, Bai X, Li S, Lei Y, Dai Q, Qin R, Wang T, Dong B, Zheng Z. and Ren X. Solvothermal Synthesis and Photoluminescent Properties of ZnS/Cyclohexylamine: Inorganic−Organic Hybrid Semiconductor Nanowires. J. Phys. Chem. B. 2006; 110(26): 12948-12953

26. Skotheim T and Elsenbaumer R Handbook of Conducting Polymers, Marcel Dekker Inc: New York; 1998.

27. 27. Vossmeyer T, Katsikas L, Giersig M, I. Popovic G, Diesner K, Chemseddine A, Eychmuller A, and Weller H. CdS Nanoclusters: Synthesis, Characterization, Size Dependent Oscillator Strength, Temperature Shift of the Excitonic Transition Energy, and Reversible Absorbance Shift. J. Phy. Chem. B. 1994; 98: 7665 -7573.

28. Klug HP and Alexander LE, X-ray diffraction procedures for polycrystalline and amorphous materials, John Wiley and Sons: New York; 1954; 491.

29. Quillard S., Louarn G., Lefrant S. and Macdiarmid A. G., Vibrational analysis of polyaniline: A comparative study of leucoemeraldine, emeraldine, and pernigraniline bases. Phys. Rev. B 1994; 50: 12496-12502.

30. Stejskal J , Sapurina I , Trchova M., Prokes J, Krivka I and Tobolkova E, Solid-State Protonation and Electrical Conductivity of Polyaniline. Macromolecules. 1998; 31: 2218-2222.

31. Macdonald JR, Impedance spectroscopy. John Wiley: New York; 1987

32. Jonscher A. K., Dielectric Relaxation In Solids. Chesla Dielectric Group: UK; 1983

33. http://www.solartonanalytical.com/downloads/downloads.html

34. Mott NF, Davis E, Electronic Process in Non Crystalline Materials. 2nd ed:, Oxford, Clarendon; 1979

35. Havriliak S. and Negami S., A complex plane representation of dielectric and mechanical relaxation processes in some polymers. Polymer. 1967; 8: 161-210